

TENSILE PROPERTIES OF BOWING NATURAL LFT COMPOSITES

Junji Noda¹, Kosuke Torii², Syotaro Hiramatsu³ and Koichi Goda⁴

¹Graduate School of Science and Technology for Innovation, Yamaguchi University,
2-16-1 Tokiwadai, Ube, Japan Email: nodaj@yamaguchi-u.ac.jp

²Graduate School of Science and Engineering, Yamaguchi University,
2-16-1 Tokiwadai, Ube, Japan Email: u031ve@yamaguchi-u.ac.jp

³Graduate School of Science and Technology for Innovation, Yamaguchi University,
2-16-1 Tokiwadai, Ube, Japan Email: w044vd@yamaguchi-u.ac.jp

⁴Graduate School of Science and Technology for Innovation, Yamaguchi University,
2-16-1 Tokiwadai, Ube, Japan Email: goda@yamaguchi-u.ac.jp

Keywords: natural fiber composites, LFT, bowing, Young's modulus, FEM

Abstract

The objective of this study is to clarify the reinforcing mechanism of bowing natural LFT composites. At first, the bowing natural fibers were classified into some patterns in geometry and investigated these distributions using the X-ray computed tomography. The bowing and inclined fibers exist near skin of the injected specimens. It was reported that in the case of glass fibers, the inclined fibers exist in core of the specimens. The difference of fiber geometry was derived from the fracture strain of fibers. Using the bowing fiber frequency distributions and classification, the Young's modulus was well predicted based on the rule of mixtures. Based on FE-analyses, more proper prediction of Young's modulus was also carried out using the proposal of equivalent fiber geometry.

1. Introduction

Discontinuous-fiber-reinforced thermoplastic composites are commercially important in engineering applications. These materials may be processed by conventional methods, such as injection molding, and offer improvements in mechanical properties over those of unfilled materials. They replace metals in various applications because of their ease of fabrication, light weight and economy. However, additional considerations include processing-induced anisotropy in terms of through-thickness fiber orientation and length within molded parts. The mechanical property of these composites results from a combination of the fiber and matrix properties and the ability to transfer stresses across the fiber-matrix interface. Variables such as the fiber content, length, diameter, orientation and the interfacial strength are of prime importance to the final balance of properties exhibited by these injection molded thermoplastic composites [1-4]. Sato et al. [2] describe the mechanism of fracture for short-fiber reinforced thermoplastic composites in detail, and proposed some methods of improving composite toughness: (i) the use of fibers with small diameters, which reduce stress concentration at fiber tips due to the closer packing of fibers; (ii) the use of longer fibers than conventional ones, these have the effect of reducing the number of fiber tips which act as stress concentrators; and (iii) the introduction of interfacial layers between the fiber and matrix.

The increasing interest in natural fibers as reinforcement of polymer-matrix composites is motivated primarily by environmental and ecological concerns; nevertheless natural fibers should also be competitive economically to ensure their application in composites. Bast fibers, such as flax and ramie, possess reasonably high mechanical properties that ensure competitiveness with traditional reinforcing fibers. Natural fibers as reinforcement for petrochemical polymers like PP (polypropylene) have already been established in the automotive industry.

The main problem on discontinuous fiber composites is that the fibers are often broken during the fabrication processes such as extrusion and injection molding, resulting in shorter fiber length than the critical one. In order to maintain appropriate mechanical properties of the composites, as mentioned above, the fiber length has to be longer than the critical one. One of popular methods is to use pultrusion technique for the manufacture of long fiber thermoplastic (LFT) composites. Thomason et al [5] also introduced a coating process using jute yarns to produce composite strands. However, poor performance of tensile properties on injection-molded composites was reported, which is caused by low level of impregnation between fibers. To solve this drawback, Bledzki et al [6] tried two-step extrusion process. Meanwhile, we developed a continuous ramie single yarn reinforced PP composite strand using a new and relatively simplified multi-pin-assisted resin impregnation (M-PaRI) process [7]. Continuous ramie single yarn/PP composites were produced through a new combined technique proposed in the previous study, which consists of resin coating process (Process A) and Multi-pin-assisted resin impregnation (M-PaRI) process (Process B) as shown in Fig.1. The continuous single yarns were first delivered via preheating process into a cross-head die attached to a Φ 15mm single screw extruder, into which PP pellets and MA-PP powders were fed at the same time. The mixed resin was coated on the single yarns in the die at Process A. After that, it can be impregnated into inter-fibers through multi-pin system at Process B.

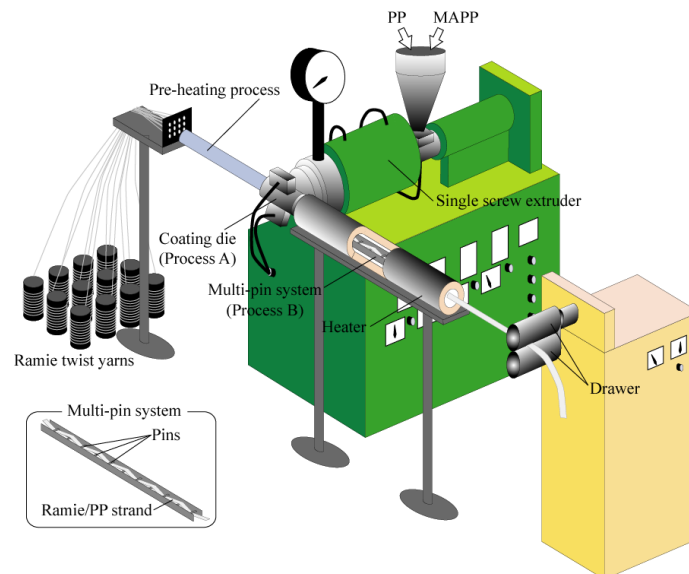
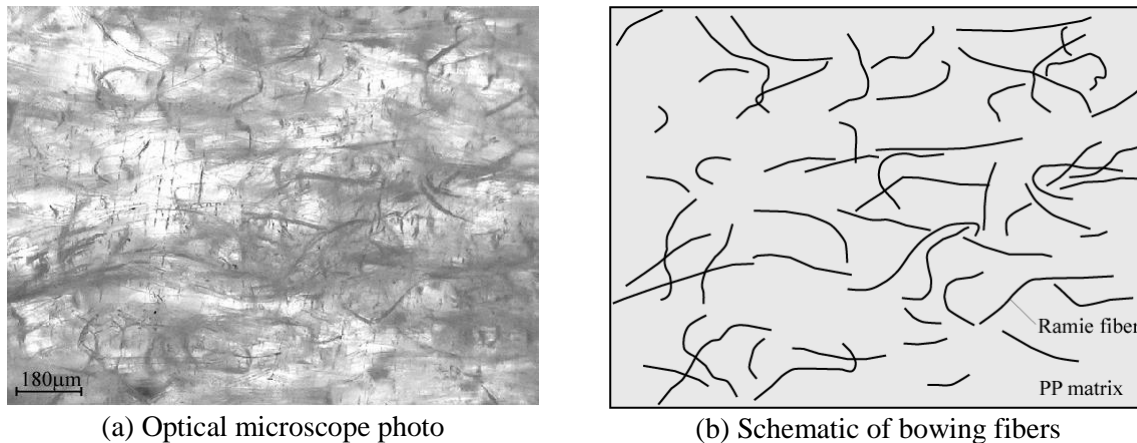


Figure 1. Schematic of M-PaRI equipment system for natural fiber composites.

Mechanical properties obtained from tensile tests using the injection-molded composites based on the pellets of our strand are good results and these results are consistent with the complete resin impregnation between fibers by means of additional Process B. In general, the two-screw extruder or kneading machine were used before injection molding for discontinuous fiber reinforced composites in order to achieve the complete resin impregnation. However, the length of almost fibers in the composites was shorter than the critical fiber length. The drastically improvements in tensile strength and Young's modulus were derived from the complete resin impregnation and the fiber length. The fiber geometry in our composites was observed by the optical microscope and it was confirmed the bowing natural fibers occurred as shown in Fig. 2. It was found that the bowing fibers due to high fracture strain of natural fibers exist and the reinforced effect and fracture mechanism of fibers would be complicated so that these fibers were interlaced.



(a) Optical microscope photo

(b) Schematic of bowing fibers

Figure 2. Bowing Ramie fibers in PP matrix

The objective of this study is to clarify the reinforcing mechanism of bowing natural LFT composites. At first, the bowing natural fibers were classified into some patterns in geometry and investigated these distributions using the staged optical microscope observations and the X-ray computed tomography. Using the bowing fiber frequency distributions and classification, the Young's modulus was predicted based on the rule of mixtures. Based on FE-analyses, more proper prediction of Young's modulus was also carried out using the proposal of equivalent fiber geometry.

2. Experiments

2.1. Materials and Specimens

Continuous ramie single yarns, having fineness of 95 tex, Type no. 16 (Tosco Co., Ltd., Japan) and polypropylene (Prime Polymer Co. Ltd., Japan) were used as reinforcement and matrix material, respectively.

It is known that high adhesion between hydrophilic fibers and hydrophobic resin by chemical bonding is induced by available OH groups on the fiber surface. The resin adheres to the fiber surface through molecular chain entanglement. During this reaction, maleic anhydride-grafted polypropylene (MA-PP) works as a coupling agent to realize such chemical bonding [8]. In this study also, MA-PP (Kayaku Akzo Co., Ltd., Japan) was used to promote a chemical interaction between the fiber and matrix.

The continuous composite strands containing six ramie yarns obtained by M-PaRI equipment system as shown in Fig. 1 were chopped to pellets of about 2mm length. The set temperature was 190°C at Process A and B. The pellets were molded into a specimen die on an injection molding machine (IMC-18D1, Imoto Machinery Co., Ltd., Japan). Then tensile specimens based on Japanese Industrial Standards, JIS K 7162, Type 5B were obtained. The dog-bone shape specimen has 3mm in width, 2mm in thickness and 18mm in gage length. The temperatures were set at 190°C for injection molding. Fiber contents of the specimens were adjusted to 5%.

2.2. Fiber Morphology

In order to investigate the fiber morphology, the polished surfaces at 0.2 mm intervals of the specimens were observed using the optical microscope. In order to confirm the fiber morphologies in 3D, X-ray computed tomography was implemented using the X-ray CT (Xradia 410 Versa, ZEISS, Germany). The fiber length and its morphology were measured on 500 fibers at the skin and core, respectively.

From the fiber length distribution in composites obtained by our method, it was found that the average fiber length was 1.6mm, and the length of 99% fibers was longer than critical length of 0.3mm. These fiber morphologies were classified to the bowing fibers with some curvatures, S-shape fibers, bended fibers with sharp angle and others, as shown in Fig.3. The frequency rate of fiber morphologies was shown in Fig.3 in the case of skin and core. Fig.4 shows the schematic of fiber morphology for natural fiber composites with many long fibers (LF) using our method compared with that for general glass fiber composites [9]. In the case of glass with short fibers, near to the skin, the glass fibers are highly orientated in the flow direction, highlighting the formation of a frozen layer, or fountain effect, of the polymer during the mold filling. On the other hand, natural LFT composites using our method has many bowing fibers at the skin because the long natural fibers could not break according to shear stress at the frozen layer due to the high fracture strain of natural fibers compared with that of glass fibers.

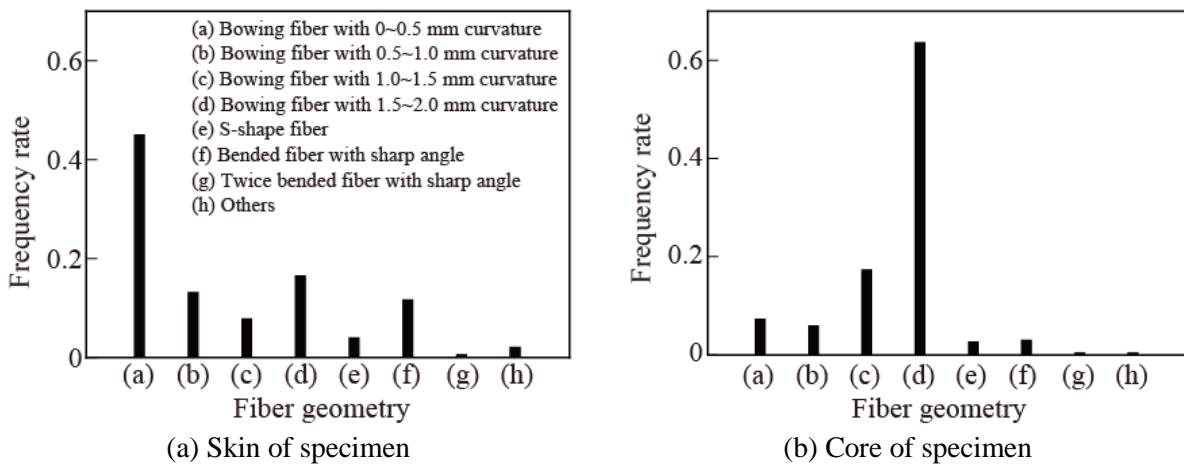


Figure 3. Bowing fiber classification and its frequency rate

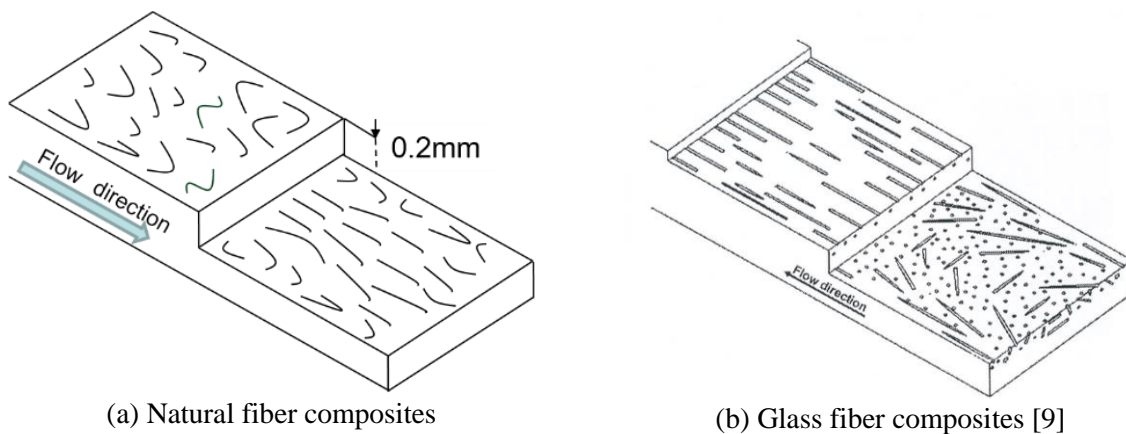


Figure 4. Schematics of fiber morphology

2.3. Tensile Tests

Tensile tests were conducted using a universal testing machine (Desktop type universal testing machine, LSC-1/30, JT Toshi Co., Ltd., Japan) at a crosshead speed of 10 mm/min. The mean cross section area of specimens was measured on three locations along the longitudinal direction, using a micrometer and then taking an average. Ten specimens were evaluated to obtain an average value. Ultimate stress, stiffness (linear region between strain 0.05% and 0.25%), and strain were determined from the stress-strain curves for each test. The obtained Young's modulus of specimen was 3.10 GPa.

3. FE Analyses

3.1. Finite Element Model

Finite element (FE) analyses were conducted in order to investigate the stress distributions of bowing fiber in the matrix. In this study the equivalent fiber geometry model which stress distributions correspond to that of continuous bowing fiber model with a curvature as shown in Fig.5-(a) was proposed, in the case for the curvature of 0.1 and 0.25 mm. This proposal model consists of three discontinuous line elements as shown in Fig.5-(c). Six nodes-2D triangle elements were used and meshes were shown in Fig.5-(b) and (d). The number of elements for fiber and matrix in model (b) and (d) were 816, 4,320, 804 and 3,302, respectively. These elements were assumed to be linear elastic isotropic body. Young's modulus and Poisson's ratio for fiber and matrix were 24.5 GPa, 1.68 GPa, 0.33 and 0.33, respectively. For the boundary conditions, three directions except for x -direction were bound in displacement, the displacement corresponding to 2% strain was applied on the other hand along x -direction.

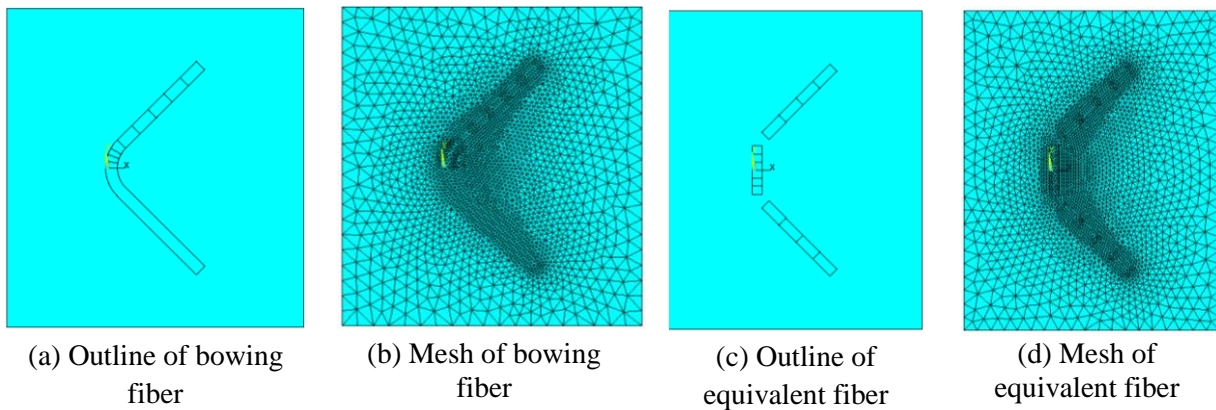


Figure 5. Finite element models

3.2. Young's Modulus Prediction

Figure 6 shows the fiber axial stress distribution transformed with fiber direction for bowing model with curvature of 0.1mm. The horizontal axis in figure 6 denoted the position from the center to the end of fiber. It was found that the fiber axial stress increases with increase of fiber angle at the range from the position of 0 to 4, on the other hand, the fiber axial stresses after the position 5 were almost constant. The fiber axial stress distributions of initial geometry fiber model as shown in figure 5-(d) was also shown in figure 6. In this study, it is assumed that the capability of fiber stress loading contributed to Young's modulus of composites depends on the fiber alignment over 45 degree along the loading direction. Based on this assumption, we adjusted the angle and length of the inclined fiber elements in figure 5-(c) to correspond with the capability of fiber stress loading for bowing model with curvature. This stress distribution for the adjusted equivalent fiber model was finally added in figure 6. In this calculation, the inclined fiber length and angle were adjusted from 0.210 mm and 45 degree in the initial model to 0.200 mm and 41.64 degree. Using the inclined initial fiber length l_L , angle θ_L , adjusted length l'_L and angle θ'_L , the correct ratio ζ_l , ζ_θ for the length and angle were defined as follows,

$$\zeta_l = l'_L / l_L, \quad \zeta_\theta = \theta'_L / \theta_L \quad (1)$$

For short fiber reinforced composites, the coefficients of fiber length $\eta'_{l,i}$ and orientation $\eta'_{\theta,i}$ for fiber i were used to predict the composite Young's modulus. These coefficients were defined as follows.

$$\eta'_{l,i} = 1 - \frac{\tanh\left(\frac{1}{2}\beta\zeta_l l_i\right)}{\frac{1}{2}\beta\zeta_l l_i}, \quad \eta'_{o,i} = \cos^2(\zeta_\theta \theta_i) \quad (2)$$

Where, l_i and θ_i are the length and orientation angle in the experimental results for fiber i , and β is below.

$$\beta = \sqrt{\frac{2G_m}{E_f r_f^2 \ln(R/r_f)}} \quad (3)$$

Where, E_f and r_f are the Young's modulus and radius of fiber, respectively. G_m is the shear modulus of matrix, and R is the average distance between fibers. As mentioned above, our natural LFT composites have the different fiber morphologies between skin and core areas, then the Young's modulus for each area E_j was calculated using the each fiber distribution in length and angle as follows.

$$E_j = \left(\sum_{i=1}^{N_j} \eta'_{l,i} \eta'_{o,i} E_f V_{f,i} \right) + E_m (1 - V_{f,j}) \quad (4)$$

Finally, the composite Young's modulus E_c was calculated based on a below equation using the volume fraction of area j , V_j .

$$E_c = \sum_{j=1}^2 E_j V_j \quad (5)$$

In this calculation, the material and geometric parameters were used as shown in Table 1. The predicted Young's modulus of natural LFT composites was 3.21 GPa and this prediction was good agreement with experimental value of 3.10 GPa. From the comparison with experiments, the validity of the equivalent fiber model in the fiber geometry was proved. It was then suggested that for the Young's modulus prediction of bowing fibers in composites, the fiber lengths and angles with over 45 degree alignment along the loading direction should be measured in experiments.

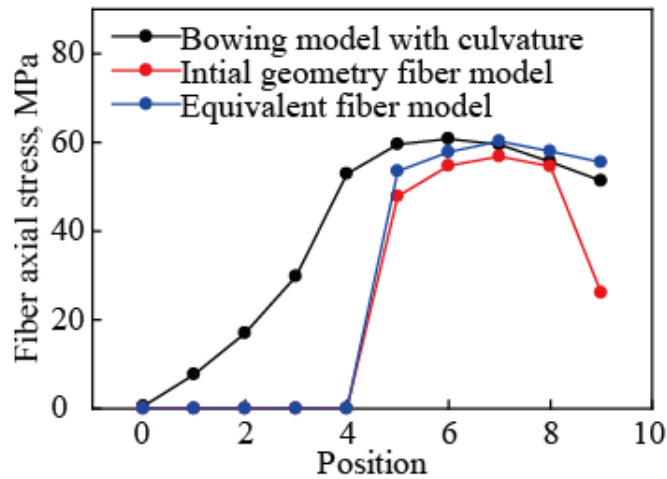


Figure 6. Fiber axial stress distributions.

Table 1. Material and geometric parameters for Young's modulus prediction

G_m [GPa]	r_f [mm]	R [mm]	V_f	V_j (core)
0.63	0.03	0.13	0.05	0.69

4. Conclusions

Based on our M-PAI process, natural LFT composites with high Young's modulus were developed. The fiber morphology in the composites was observed by the optical microscope and it was confirmed the bowing natural fibers occurred. From 500 measurements, it was found that natural LFT composites has many bowing fibers at the skin because the long natural fibers could not break according to shear stress at the frozen layer in mold due to the high fracture strain of natural fibers compared with that of conventional glass fibers.

FE analyses were conducted in order to predict the Young's modulus of natural LFT composites with bowing fibers. The equivalent fiber model in geometry was proposed and the Young's modulus prediction was compared with experiments. Consequently, it was then suggested that for the Young's modulus prediction including bowing fibers in composites, the fiber lengths and angles with over 45 degree alignment along the loading direction should be measured in experiments.

Acknowledgments

This work was supported by JSPS KAKENHI Grant Number 26709003.

References

- [1] N. Sato, T. Kurauchi, S. Sato and O. Kimigaito, Mechanism of fracture of short glass fiber-reinforced polyamide thermoplastic, *J. Mater. Sci.*, 19: 1145-1152, 1984.
- [2] N. Sato, T. Kurauchi, S. Sato and O. Kimigaito, Microfailure behavior of randomly dispersed short fiber reinforced thermoplastic composites obtained by direct SEM observation", *J. Mater. Sci.*: 26, 3891-3898, 1991.
- [3] J.L. Thomason, The influence of fiber properties of the performance of glass fiber-reinforced polyamide 6.6, *Comp. Sci. Tech.*: 59, 2315-2328, 1999.
- [4] J.L. Thomason, The influence of fiber length, diameter and concentration on the impact performance of long glass-fiber reinforced polyamide 6.6, *Comp. A*: 40, 114-124, 2009.
- [5] J.L. Thomason, Dependence of interfacial strength on the anisotropic fiber properties of jute reinforced composites, *Polymer Composites*, 31: 1525-1534, 2010.
- [6] A.K. Bledzki, A. Jaskiewicz and D. Scherzer, Mechanical properties on PLA composites with man-made cellulose and abaca fibers, *Comp. A*: 40, 404-412, 2009.
- [7] H.B. Kim, S. Kimura, K. Goda, J. Noda and K.Aoki, A new method for continuous production of ramie yarn reinforced composites, *proceedings of 15th European Conference on Composite Materials ECCM-15, Venice, Italy, June 25-28 2012*.
- [8] G. W. Beckermann and K. L. Pickering, Engineering and evaluation of hemp fibre reinforced polypropylene composites: fibre treatment and matrix modification, *Comp. A*, 39, 6: 979-988, 2008.
- [9] A. Bourmaud, G. Ausias, G. Lebrun, M.-L. Tachon and C. Baley, Observation of the structure of a composite polypropylene/flax and damage mechanisms under stress, *Industrial Crops and Products*, 43: 225-236, 2013.